Tailoring diffraction-induced light distribution toward controllable fabrication of suspended C-MEMS

Hu Long,[1] Shuang Xi,[1] Dan Liu,[1] Tielin Shi,[2] Qi Xia,[2] Shiyuan Liu,[2] and Zirong Tang[1,2,*]

[1] *Wuhan National Laboratory for Optoelectronics, Huazhong University of Science and Technology, Wuhan 430074, China*

[2] *State Key Laboratory of Digital Manufacturing Equipment and Technology, Huazhong University of Science and Technology, Wuhan 430074, China*

[*] *zirong@mail.hust.edu.cn*

Abstract: A simple and controllable method is proposed to fabricate suspended three-dimensional carbon microelectromechanical systems (C-MEMS) structures by tailoring diffraction-induced light distribution in photolithography process. An optical model is set up and the corresponding affecting parameters are analyzed to interpret and predict the formation of suspended structures based on Fresnel diffraction theory. It is identified that mask pattern dimensions, gap distance between the photomask and photoresist, and the exposure time are critical to the final suspended structures, which have also been verified through experimental demonstrations. The fabricated biocompatible suspended C-MEMS structures could find wide applications in electrochemical and biological areas.

©2012 Optical Society of America

OCIS codes: (050.6875) Three-dimensional fabrication; (220.4000) Microstructure fabrication; (050.1940) Diffraction.

References and Links

1. C. L. Wang, G. Y. Jia, L. Taherabadi, and M. Madou, "A novel method for the fabrication of high-aspect ratio C-MEMS structures," J. Microelectromech. Syst. **14**(2), 348–358 (2005).
2. B. Y. Park, L. Taherabadi, C. L. Wang, J. Zoval, and M. Madou, "Electrical properties and shrinkage of carbonized photoresist films and the implications for carbon microelectromechanical systems devices in conductive media," J. Electrochem. Soc. **152**(12), J136–J143 (2005).
3. D. B. Burckel, C. M. Washburn, A. K. Raub, S. R. J. Brueck, D. R. Wheeler, S. M. Brozik, and R. Polsky, "Lithographically defined porous carbon electrodes," Small **5**(24), 2792–2796 (2009).
4. C. L. Wang, L. Taherabadi, G. Y. Jia, M. Madou, Y. Yeh, and B. Dunn, "C-MEMS for the manufacture of 3D microbatteries," Electrochem. Solid-State Lett. **7**(11), A435–A438 (2004).
5. W. Chen, M. Beidaghi, V. Penmatsa, K. Bechtold, L. Kumari, W. Z. Li, and C. L. Wang, "Integration of carbon nanotubes to C-MEMS for on-chip supercapacitors," IEEE Trans. Nanotechnol. **9**(6), 734–740 (2010).
6. H. Xu, K. Malladi, C. L. Wang, L. Kulinsky, M. Song, and M. Madou, "Carbon post-microarrays for glucose sensors," Biosens. Bioelectron. **23**(11), 1637–1644 (2008).
7. A. Campo and C. Greiner, "SU-8: a photoresist for high-aspect-ratio and 3D submicron lithography," J. Micromech. Microeng. **17**(6), R81–R95 (2007).
8. B. Meliorisz and A. Erdmann, "Simulation of mask proximity printing," J. Micro/Nanolith. MEMS MOEMS. **6**, 023006 (2007).
9. W. J. Kang, E. Rabe, S. Kopetz, and A. Neyer, "Novel exposure methods based on reflection and refraction effects in the field of SU-8 lithography," J. Micromech. Microeng. **16**(4), 821–831 (2006).
10. Y. J. Chuang, F. G. Tseng, and W. K. Lin, "Reduction of diffraction effect of UV exposure on SU-8 negative thick photoresist by air gap elimination," Microsyst. Technol. **8**(4-5), 308–313 (2002).
11. R. Yang and W. J. Wang, "A numerical and experimental study on gap compensation and wavelength selection in UV-lithography of ultra-high aspect ratio SU-8 microstructures," Sens. Actuators B Chem. **110**(2), 279–288 (2005).
12. Y. Cheng, C. Y. Lin, D. H. Wei, B. Loechel, and G. Gruetzner, "Wall profile of thick photoresist generated via contact printing," J. Microelectromech. Syst. **8**(1), 18–26 (1999).
13. Z. R. Tang, T. L. Shi, J. Gong, L. Nie, and S. Y. Liu, "An optimized process for fabrication of high-aspect-ratio photoresist-derived carbon microelectrode array on silicon substrate," Thin Solid Films **518**(10), 2701–2706 (2010).

#168827 - $15.00 USD Received 18 May 2012; revised 4 Jul 2012; accepted 10 Jul 2012; published 12 Jul 2012

14. K. Malladi, C. L. Wang, and M. Madou, "Fabrication of suspended carbon microstructures by e-beam writer and pyrolysis," Carbon **44**(13), 2602–2607 (2006).
15. K. Y. No, G. D. Kim, and G. M. Kim, "Fabrication of suspended micro-structures using diffsuser lithography on negative photoresist," J. Mech. Sci. Technol. **22**(9), 1765–1771 (2008).
16. C. S. Sharma, H. Katepalli, A. Sharma, and M. Madou, "Fabrication and electrical conductivity of suspended carbon nanofiber arrays," Carbon **49**(5), 1727–1732 (2011).
17. N. R. Franklin, Q. Wang, T. W. Tombler, A. Javey, M. Shim, and H. J. Dai, "Integration of suspended carbon nanotube arrays into electronic devices and electromechanical systems," Appl. Phys. Lett. **81**(5), 913–915 (2002).
18. M. Born and E. Wolf, *Principles of Optics* (Cambridge University Press, 2003), Chap. 1, 2, 7, 8.
19. M. Bass and V. N. Mahajan, *Handbook of Optics* (McGraw-Hill, 2010), Volume I, Chap. 1–3.
20. M. Gaudet, J. C. Camart, L. Buchaillot, and S. Arscott, "Variation of absorption coefficient and determination of critical dose of SU-8 at 365 nm," Appl. Phys. Lett. **88**(2), 024107 (2006).

1. Introduction

Recently, three-dimensional (3D) C-MEMS structures consisting of high aspect-ratio carbon microelectrodes have drawn much attention due to their good mechanical, electrical, electrochemical properties and excellent biocompatibility [1–3]. These microelectrodes derived from thick photoresist can be used for various miniaturized carbon-based devices such as micro-batteries, super-capacitors and biosensors [4–6].

The fabrication process of C-MEMS structures with high aspect-ratio mainly includes two steps, lithography and pyrolysis process, where thick photoresist micropatterns created in lithography process are transformed into amorphous glassylike carbon microstructures under high temperature and inert atmosphere. The lithography process as a mature fabrication technique has been widely studied both experimentally and theoretically [7]. Optical simulations of diffraction effects for the lithography process has been shown that mask-induced diffraction effects may affect the accuracy of micropatterns [8]. Investigations have also been conducted to reduce diffraction-induced negative effects such as avoiding negatively sloped sidewall profiles of 3D micropatterns in the lithography of SU-8 photoresist [9–11]. It was shown that smaller and uniform gap between photomask and the photoresist could reduce the diffraction-induced error [12]. Meanwhile, suspended carbon microstructures have been observed through extended exposure duration in the lithography [1,13], which could be due to the diffraction effects. However the underlying formation mechanism of the suspended structure has not been explored yet.

On the other hand, it was reported that suspended structures are free of any intermolecular or surface interactions with the substrate, which can be used for mechnical, electrical, and electrochemical measurements or the development of carbon-based novel microdevices [1,14–17]. It has been reported that suspended structures could be obtained through E-beam writer, diffuser lithography and interference lithography followed by pyrolysis process [14–16]. In present study, we report our efforts to develop a simple, low-cost and controllable method to fabricate suspended C-MEMS structures. The process is developed by taking advantage of diffraction effects, which were usually tried to be avoided in conventional lithography process. Firstly, an optical model based on Fresnel diffraction theory will be set up for lithography process. Then, critical mask design and process paramters will be identified through simulation to predict the formation of suspended structures. The fabrication experiments of various suspended structures will be conducted to verify the theoretical analysis. In the end, a controllable methodology will be proposed for the fabrication of suspended C-MEMS structures.

2. Optical modeling and simulation

2.1 The optical model in UV lithography

During the lithography process, exposure process and photomask will define the final patterns. Therefore, we establish a model based on Fresnel diffraction resulted from the air gap between the photomask and photoresist to simulate the light intensity distribution on the top surface of photoresist in exposure process. In Fig. 1(a), a typical mask design is schematically shown for the fabrication of micropost arrays with negative photoresist, where

#168827 - $15.00 USD Received 18 May 2012; revised 4 Jul 2012; accepted 10 Jul 2012; published 12 Jul 2012
(C) 2012 OSA

a and d are the diameter of aperture and center distance between two apertures respectively. In Fig. 1(b), the schematic drawing of light propogation in lithography process is presented, where the mask is illuminated with a vertically incident plane wave at the wavelength of 365 nm. The light source is designed to provide uniform monochromatic illumination over the entire mask object. $E(P_1)$ is the light wave amplitude at point P_1 on the mask and $E(P_1)$ is constant. The incident light is completely coherent. In our simulation, the incident light intensity is 5 mW/cm^2 according to the experiment condition. The distance between the photomask and the photoresist is several microns for proximity lithography. In Fig. 1(c), a 3-dimensional coordinate system is set up based on Fig. 1(b). The mask plane is called as plane (x_1, y_1) which means the coordinate of arbitrary point P_1 in this plane is (x_1, y_1). The surface of photoresist is called plane (x, y) and the coordinate of arbitrary point P is (x, y). We define the axis perpendicular to both plane (x_1, y_1) and plane (x, y) as the axis Z.

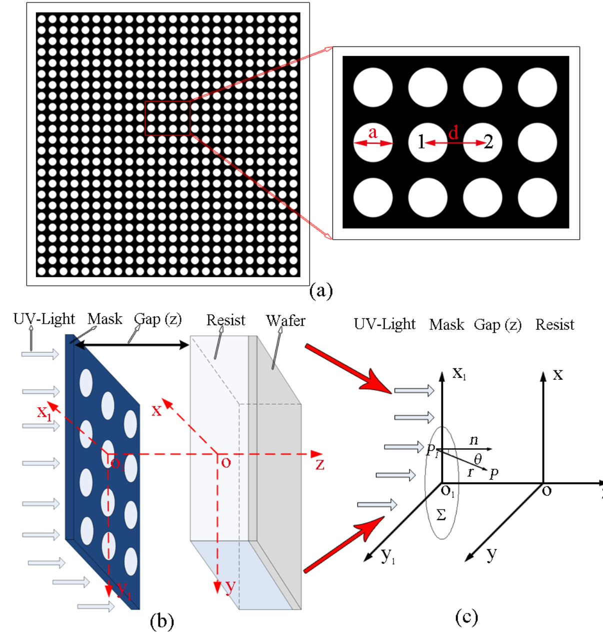

Fig. 1. Schematic drawing of the photomask and modeling of light transmision in lithography: (a). Design of the mask pattern; (b). Schematics of the lithography process; (c). 3D coordinates in light transmmision modeling.

Depending on the Rayleigh-Sommerfeld diffraction formulation [18,19], the amplitude at point P on the top surface of photoresist is

$$E(P)=\frac{1}{j\lambda}\iint_{\Sigma}E(P_1)\frac{\exp(jkr)}{r}\cos\theta ds \qquad (1)$$

Where $k = 2\pi/\lambda$, λ is the wavelength of incident UV light, and r represents the distance between P and P_1. θ is the angle between PP_1 and the axis Z. Domain of intergration Σ is the aperture region which can be defined by the diameter of the aperture a.

With the paraxial approximation and Fresnel approximation, Eq. (1) can be simplified as the following:

#168827 - $15.00 USD Received 18 May 2012; revised 4 Jul 2012; accepted 10 Jul 2012; published 12 Jul 2012
(C) 2012 OSA

$$E(P) = \frac{1}{j\lambda} \iint_{\Sigma} E(P_1) \frac{\exp\left\{ jkz_0 + \frac{jk\left[(x-x_1)^2 + (y-y_1)^2\right]}{2z_0} \right\}}{z_0} dx_1 dy_1 \quad (2a)$$

where z_0 is the vertical distance between the photomask and the top surface of the photoresist, which means z_0 is equal to the air gap. As $exp(jkz_0)$, $E(P_1)$ and z_0 are constant, Eq. (2a) can be rewritten as:

$$E(P) = \frac{\exp(jkz_0) E(P_1)}{j\lambda z_0} \iint_{\Sigma} \exp\left\{ \frac{jk\left[(x-x_1)^2 + (y-y_1)^2\right]}{2z_0} \right\} dx_1 dy_1 \quad (2b)$$

As the aperture array distribution is symmetrical, we choose the typical pattern including twelve apertures as shown in Fig. 1(a) to discuss the light intensity distribution between two adjacent apertures, and apeture 1 is defined as the center aperture. Assuming that all monocharomatic waves are superposed at some point *P*, the electromagnetic field at point *P* is:

$$\begin{aligned} E^{'}(x,y) = {} & E(x,y) + E(x+d,y) + E(x-d,y) + E(x,y+d) + E(x+d,y+d) + \\ & E(x+d,x-d) + E(x-d,y+d) + E(x-2d,y+d) + E(x-d,y-d) \\ & + E(x-2d,y) + E(x-2d,y+d) + E(x-2d,y-d) \end{aligned} \quad (3)$$

And the light intensity distribution on top surface of the photoresist can be expressed as:

$$I(x,y) = \left| E^{'}(x,y) \right|^2 \quad (4)$$

2.2 The energy threshold model

The total energy applied on the top surface of the photoresist is

$$E = I(x,y) \times t \quad (5)$$

Where *t* is exposure time.

Here, to release the reaction in the photoresist, a reactive energy E_0 is necessary, which is strongly dependent on the properties of photoresist.

If $E \geq E_0$, photoresist will get enough energy to release the reaction and become a solid form.

If $E \leq E_0$, the photoresit will be removed in development process.

The key in the fabrication of suspended C-MEMS structures is the Fresnel diffraction that gives more energy to the outskirt of mask patterns. In normal exposure time, the light intensity distribution caused by the diffraction effects is generally weak, which means *E* is usually less than E_0. Through the increase of exposure time, the surface layer of the photoresist outside the aperture absorbs enough energy from diffraction light to overcome the threshold E_0 and react into solid state. As described by Gaudet et al, the absorption of thick-films of the negative photoresist SU-8 is strong during photolithographic exposure by UV light (365 nm) [20]. Their study results show that the SU-8 becoming more absorbing as the exposure time increases, which means that small light energy E brought by diffraction effects will be absorbed only by the surface layer of the SU-8 even if overexposure were applied to the SU-8 photoresist.

In the following paragraph, we will analyze the factors affecting the light intensity distribution through simulation.

#168827 - $15.00 USD Received 18 May 2012; revised 4 Jul 2012; accepted 10 Jul 2012; published 12 Jul 2012
(C) 2012 OSA

2.3 Light intensity distribution simulation

Numerical simulations are conducted to study the effects of various paramters on light intensity distribution on the top surface of photoresist. According to Eq. (2-4), the intensity distribution can be obtained by choosing air gap and mask pattern dimensions. As shown in Fig. 2(a), 3D light intensity distribution pattern on the top surface of photoresist is illustrated, where the air gap is 300 μm, the diameter of apertures *a* is 20 μm, and the center distance *d* is 40 μm. Figure 2(b) shows the top view of Fig. 2(a), demonstrating that the diffraction effects lead to light intensity distribution outside the mask window as region A and region B indicated, while region C shows the light distribution from the aperture. Comparing with region B, region A has a stronger and more continuous light intensity distribution. In this situation, the light intensity of region A is around 0.2 to 1.0 mW/cm^2, region B is 0 to 0.4 mW/cm^2 and region C is 1 to 20 mW/cm^2. After exposure, region C absorbs enough energy to form the post. The energy at region A could be only absorbed by the surface layer completely due to the relatively week intensity, and thus to ensure the top layer preserved during development to form suspended ribbon. The region B having isolated "islands" in energy distribution will be removed after development.

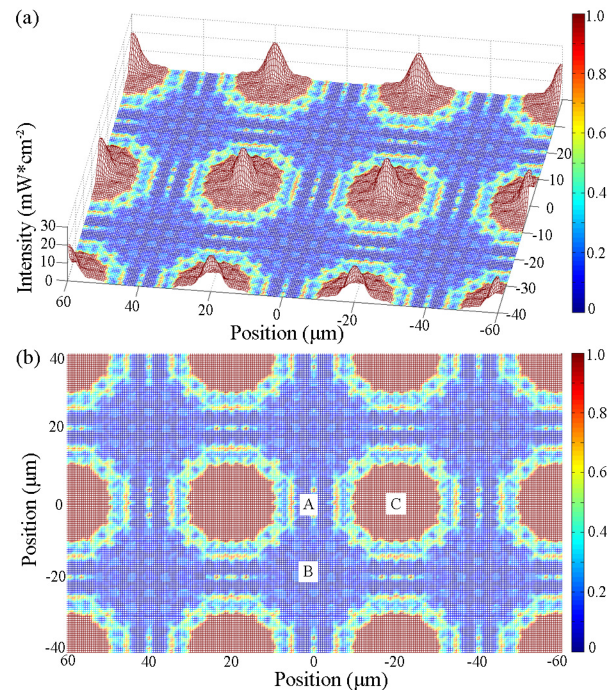

Fig. 2. (a). Typical simulation result of 3D light intensity distribution patterns on the top surface of photoresist with the air gap distance of 300 *μm*. (b). Top view of Fig. 2(a) with color indicating the light intensity distribution on the top surface of photoresist.

In order to analyze the effects of air gap and mask patterns on the light intensity distribution, we intercept the light intensity distribution between two neighboring apertures. In this simulation the mask pattern is fixed with the *a* of 20 μm and the *d* of 40 μm. As shown in Fig. 3(a), various intensity distribution patterns on the top surface of photoresist depending on the air gap are schematically illustrated. Figure 3(b) is the partial enlargement of Fig. 3(a) between the neighboring mask edges shown from −10 μm to 10 μm. The average intensity between two mask edges is also shown in Fig. 3(b), which is calculated by the following formula:

$$I_{ave} = \frac{\int Idl}{l} = \frac{\int Idl}{d-a} \tag{6}$$

It can be observed from the magnified view in Fig. 3(b), the intensity distribution curve between two mask edges shows an obvious trend: Light intensity between two neighboring edges increases with the increasing of gap diatance in general. And this can also be confirmed by the comparison of average intensity between the neighboring mask edges. When z_0 is 300 um, the average intensity is 0.3715 mW/ cm^{-2}, showing a great increase compared to the average value of 0.2567 mW/cm^{-2} at the air gap of 100 µm. It is suggested that the suspended structures appear easier with the increasing gap size.

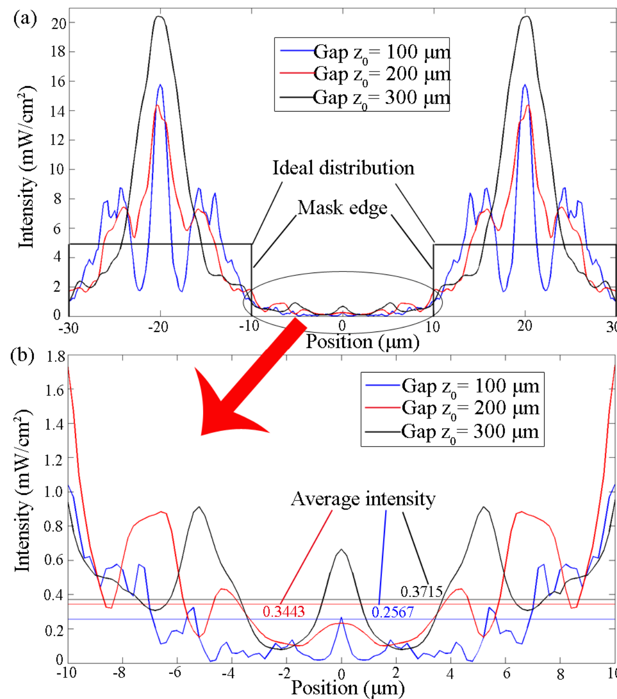

Fig. 3. (a). Simulated light intensity distribution patterns on the top surface of photoresist depending on air gap; (b). Partial enlargement of Fig. 3(a) with the comparision of average intensity between two mask edges.

Figure 4 shows the average intensity between two mask edges depending on the edge-to-edge distance (*d-a)* with a fixed diameter. The average intensity shows a declined trend with the increasing of the edge-to-edge distance. It is suggested that the suspended structures appear easier as we decrease the edge-to-edge distance in the mask design. As in the same edge-to-edge distance, the average intensity gets larger with the increasing of air gap, which also confirms the simulated results shown in Fig. 3.

#168827 - $15.00 USD Received 18 May 2012; revised 4 Jul 2012; accepted 10 Jul 2012; published 12 Jul 2012
(C) 2012 OSA

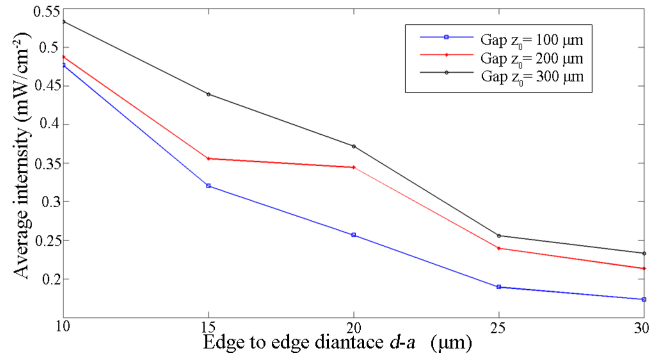

Fig. 4. The average light intensity between two neighboring mask edges depending on edge-to-edge distance at different air gaps and a fixed diameter *a*.

3. Experimental results and discussions

3.1. Experimental details

Two types of mask are designed with different aperature diameter *a* and center-to-center distance *d*, where one type is with the *a* of 30 μm and *d* of 50 μm, and the other is with the *a* of 20 μm and *d* of 40 μm. Typical lithography process for SU-8 (GM1075) was described in many literaures [1,13], and the process parameters are followed with the material's recommendations. The exposure is performed by a Karl Suss MA-6 mask aligner under UV light (365 nm) at the light intensity of 5 mW/cm^2. During the exposure, the air gap between the mask and the photoresist surface is adjusted to investigate the effect of gap distance on the formation of suspended structures. The exposure duration is also adjusted to explore the effects of exposure time on the formed structures. We have conducted the experiments with different air gaps of 0, 50 μm, 150 μm and 300 μm respectively, and the exposure duration has been controlled to be 80 s, 100 s, 120 s, 150 s, 180 s and 200 s respectively. The conversion of photoresist pattern into glassy-like carbon pattern has been realized in a quartz furnace following a typical two-step pyrolysis process [13]. The samples are characterized by Scanning Electron Microscope (SEM), and the results are presented in the following.

3.2. Results and discussion

Figure 5 shows the SEM photographs of samples resulted from the gap distance of 0, 50 μm, 150 μm and 300 μm respectively with the fixed exposure time of 120 s, where the mask is with the *a* of 30 μm and the *d* of 50 μm. Figure 5(a) exhibits conventional SU-8 pillars, while Fig. 5(b) shows the slight connection between two pillars. Obvious suspended structure appeares with the gap distance of 150 μm as shown in Fig. 5(c), in which ununiformity and fracture still exist. When the gap distance is increased to 300 μm, extraordinary uniform and regular suspended structure is obtained as shown in Fig. 5(d). It can be interpreted that suspended structure would be easier to be created with larger air gap distance, which is in consistent with the theoretical analysis and simulation results presented previously. Comparing with a typical exposure time of 80 s, the exposure duration of 120 s gives more energy to the photoresist out of the mask edge. Larger air gap will increase the diffraction effects, leading to the increase of the light intensity out of the mask window. The enough enegy absorbed by the surface layer of photoresist will initate the reaction of photoresist out of the mask window to form suspended structures.

#168827 - $15.00 USD Received 18 May 2012; revised 4 Jul 2012; accepted 10 Jul 2012; published 12 Jul 2012
(C) 2012 OSA

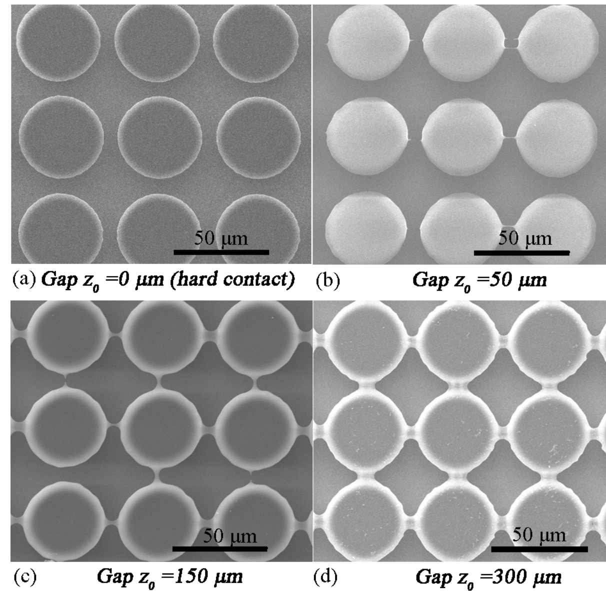

Fig. 5. SEM photographs of SU-8 patterns formed after exposure time of 120 s under various air gap z_0: (a) hard contact; z_0 = 0 μm; (b) z_0 = 50 μm; (c) z_0 = 150 μm; (d) z_0 = 300 μm.

Figure 6 shows SEM images of samples with different exposure time. The results are obtained with the diameter of the aperture of 20 μm, the center-to-center distance of 40 μm and the fixed gap size of 300 μm. Figure 6(a) shows the conventional SU-8 pillars with the expoure time of 80 s. Figure 6(b), 6(c), 6(e), 6(f) and 6(g) show the suspended structures with the exposure time of 100 s, 120 s, 150 s, 180 s and 200 s respectively, while Fig. 5(d) and (h) show the side views of the suspended patterns for the exposure time of 120 s and 200 s respectively. When the exposure time is slightly exteneded to 100 s from the normal exposure time of 80 s, overhanging in the pillars but not all connected with each other can be observed. As we keep increasing the exposure time, it exhibits suspended network structures that each pillar is connected with the surrounding pillars in a more stable way. It is obvious that increasing exposure time exhibits suspended networks with larger connecting width and thickness, which can form the complete suspended film in the end as shown in Fig. 6(g). From Fig. 6, we can also observe that the thickness and width of the ribbon decrease all the way from edge of the pillars to the center of egde-to-edge. The results are also in consistent with the previous theoretical predictions. The energy threshold can be met through prolonged exposure time as long as the existence of the diffraction effects during the lithography process, where longer exposure time gives more applied energy to the photoresist out of mask window edge to release the reaction of the surface. Comparing Fig. 5(d) (the aperture diamter of 30 μm) with Fig. 6(c) (the aperature diamter of 20 μm), the suspended ribbon width is increased with the decrease of the diamter at the same air gap, exposure time and edge-to-edge distance.

Due to the large air gap and small diameter of the apertures, the superposed intensity distribution of diffraction effects is perfect for the formation of suspended networks. Significant longer exposure time offers enough energy to form suspended patterns, since the energy brought by diffraction effects can just be absorbed only by the surface layer and overcome the energy threshold. Unexposed photoresist and photoresist under surface layer are taken away during the development. In a word, after getting a perfect intensity distribution through a good combination of air gap and mask patterns, prolonged exposure is the key factor to create the suspended structures.

#168827 - $15.00 USD Received 18 May 2012; revised 4 Jul 2012; accepted 10 Jul 2012; published 12 Jul 2012
(C) 2012 OSA

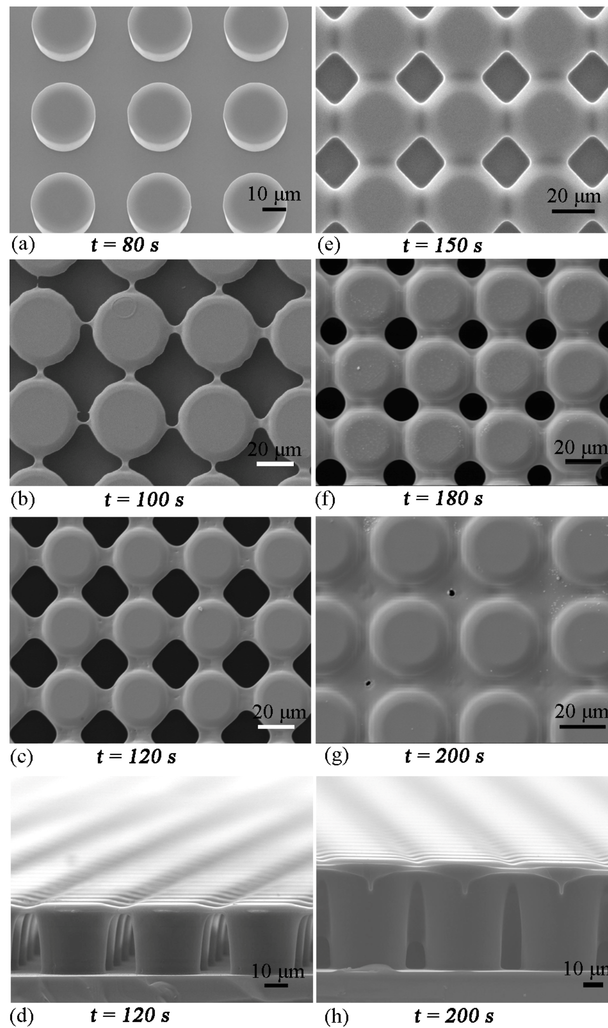

Fig. 6. SEM images of SU-8 patterns with different exposure time t: (a) t = 80 s; (b) t = 100 s; (c) t = 120 s; (d) sidewall of the SU-8 pattern in Fig. 6(c); (e) t = 150 s; (f) t = 180 s; (g) t = 200 s; (h) sidewall of the SU-8 pattern in Fig. 6(g).

Figure 7(a) and 7(b) show typical suspended ribbon structures before and after pyrolysis respectively, while Fig. 7(c) and 7(d) show typical suspended network structures before and after pyrolysis respectively. During pyrolysis, the non-carbon species in the resist polymer backbone are removed, while the bulk of the carbon remains. The patterned structures undergo significant shrinkage, but remarkably maintain their morphology and adhesion to the substrate. The structure in Fig. 7(a) is created by the exposure time of 100 s with the air gap of 300 μm and followed by shaking the developer in one-direction to crack of photoresist ribbon in the same direction during the development process. The carbon ribbon fibers obtained through uniform shrinkage in pyrolysis process is submicron as shown in Fig. 7(b) with a amplified view. Through the control of exposure time, the size of suspended carbon fibers can be controlled, however, its thickness is decreasing all the way from edge of the pillars to the egde-to-edge center. The phenomenon might be due to that the initial SU-8 pattern is in the silimar shape and the pattern is further enhanced by pyrolysis-induced shrinkage. These suspended carbon structures will offer new design platforms in the development of novel energy or sensing devices and systems since the suspended structure

#168827 - $15.00 USD Received 18 May 2012; revised 4 Jul 2012; accepted 10 Jul 2012; published 12 Jul 2012
(C) 2012 OSA

can be used as interconnects or integration components between high aspect-ratio carbon electrodes.

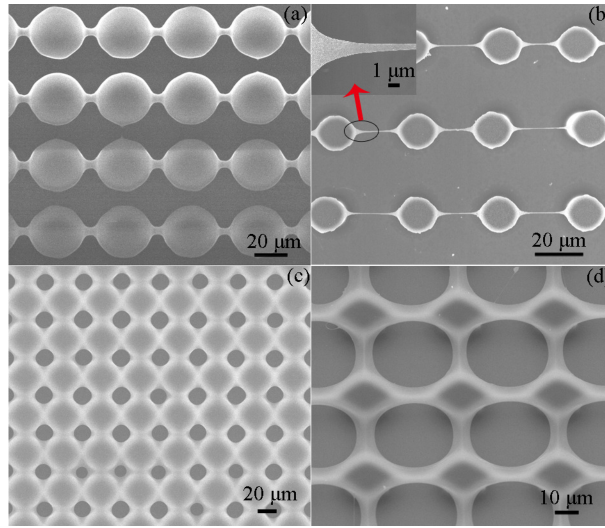

Fig. 7. SEM photographs of suspended structures: (a), (c) SU-8 before pyrolysis; (b), (d) C-MEMS structures after pyrolysis.

4. Conclusion

A simple and controllable approach for fabricating suspended C-MEMS has been developed by tailoring diffraction-induced light distribution. An optical model based on diffraction effects is set up to simulate the thick photoresist lithography process, which can be used to intepret the formation mechansim of suspended structures. Simulation results indicate that the mask pattern dimensions and gap distance are key factors affecting the light intensity distribution on the top surface of the photoresist induced by diffraction effects. By controlling the prolonged exposure time, the gap distance and proper mask design, various suspended micropatterns can be obtained, which are in consistent with the theoretical predictions. These fabricated photoresist patterns can be converted into suspended C-MEMS through pyrolysis for a variety of energy and sensing applications.

Acknowledgments

This work is financially supported by National Science Foundation of China (No. 90923019, 50875103, and 51175210) and National Key Basic Research Special Fund of China (Grant no. 2009CB724204).

#168827 - $15.00 USD Received 18 May 2012; revised 4 Jul 2012; accepted 10 Jul 2012; published 12 Jul 2012
(C) 2012 OSA